Preliminary Design of the Vacuum System for FAIR Super FRS Quadrupole Magnet Cryostat

J. Akhter, G. Pal, A. Datta, P. R. Sarma, U. Bhunia, S. Roy, S. Bhattacharyya, C. Nandi, C. Mallik and R. K. Bhandari

Variable Energy Cyclotron Center, Kolkata, India

javed.akhter@vecc.gov.in

Abstract. The Super-Conducting Fragment Separator (Super FRS) of the Facility for Antiproton and Ion Research (FAIR) at GSI Darmstadt is a large-acceptance superonducting fragment separator. The separator consists of large dipole, quadrupole and hexapole superconducting magnets. The long quadrupole magnet cryostat houses the helium chamber, which has the magnet iron and NbTi superconducting coil. The magnet weighs about 30 tons. The helium chamber is enclosed in vacuum inside the magnet cryostat. Multilayer Insulation (MLI) will be wrapped around the thermal shield to reduce radiation loss. Polyster of MLI comprises the major component responsible for outgassing. In order to reduce outgassing, pumping at elevated temperatures has to be carried out. In view of the large size and weight of the magnet, a seal off approach might not be operationally feasible. Continuous pumping of the cryostat has also been examined. Pump has been kept at a distance from the magnet considering the effect of stray magnetic fields. Oil free turbo molecular pump and scroll pump combination will be used to pump down the cryostat. The ultimate heat load of the cryostat will be highly dependent on the pressure attained. Radiation and conduction plays an important role in the heat transfer at low temperatures. This paper presents the vacuum design of the long quadrupole magnet cryostat and estimates the heat load of the cryostat.

1. Introduction

The Superconducting Fragment Separator (Super FRS) of the Facility for Antiproton and Ion Research (FAIR) at GSI in Darmstadt is a large-acceptance superconducting fragment separator to efficiently separate rare isotopes. The seperator consists of large dipole, quadrupole and hexapole superconducting magnets.

The long quadruple magnet [1, 2] along with helium chamber is housed inside a vacuum chamber. The pump has been kept at a distance from the magnet considering the effect of stray magnetic fields. Oil free turbo molecular pump and scroll pump combination will be used to pump down the cryostat. Figure 1 shows the overall view of the quadrupole magnet cryostat.

Heat transfer through Multilayer Layer Insulation (MLI) in cryostats has been elaborately studied [3-5]. C. K. Krishnaprakas [3] has considered four models for the calculation of heat flux through MLI: (1) conductance model, (2) effective emittance model, (3) conduction radiation model, (4) Connington and Tien model [4]. These models use average properties to obtain the overall heat transfer. Cunnington has considered heat transfer through each layer of MLI.

Heat transfer between the vacuum vessel at 300K and the radiation shield at 80K through each layer of MLI and the requirement of the pumping speed has been evaluated in this paper. The cryostat

vacuum system is designed to satisfy the vacuum requirement inside the cryostat and the overall pumping system is proposed.

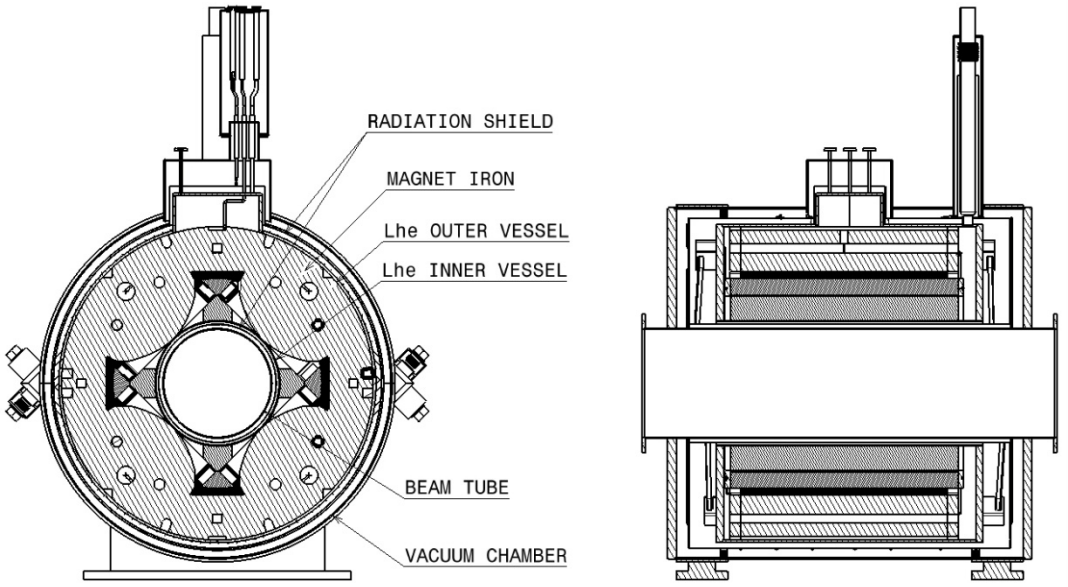

Fig. 1. Cross sectional view of the FAIR Super FRS quadrupole cryostat

2. Heat Transfer between cryostat and the radiation shield

In the quadrupole magnet, the coil will be at liquid helium temperature. A liquid nitrogen cooled radiation shield will be placed between magnet coil at 4.2 K and cryostat at 300 K. The radiation shield will be covered with MLI for reducing heat load on the liquid nitrogen system and the liquid helium system. Heat leak to the radiation shield is by radiation, gas conduction and conduction through the supports.

2.1. Numerical Model

The heat transfer due to gas conduction in molecular flow region and radiation is calculated using equations (1) [5, 6] and (2) [7]. A MATLAB code is written to solve equations (8) and (9). The code uses iterative method to calculate the resistance to heat transfer using assumed temperatures of the MLI layers. These calculated resistances were then used to find the total heat transfer rate and corrected temperatures. The calculation proceeds till there is no appreciable correction in the temperatures.

$$Q_{cond} = \alpha\left(\frac{\gamma+1}{\gamma-1}\right)p_{ins,i}\sqrt{\frac{R}{8\pi T_{ins}}}\left(T_{i+1}-T_i\right)A_{i+1} \tag{1}$$

$$Q_{rad} = \sigma A_i\left(T_{i+1}^4 - T_i^4\right)\Big/\left[\frac{1}{\varepsilon_i}+\frac{A_i}{A_{i+1}}\left(\frac{1}{\varepsilon_{i+1}}-1\right)\right] \tag{2}$$

$$\alpha = \frac{\alpha_i\alpha_{i+1}}{\alpha_{i+1}+\alpha_i\left(1-\alpha_{i+1}\right)A_i/A_{i+1}} \tag{3}$$

where α is the accommodation coefficient for copper thermal shield and cryostat wall, γ is c_p/c_v, the specific heat ratio of the gas, $p_{ins,i}$ is the interstitial pressure of insulation gas pressure, T_{ins} is the effective temperature of the non equilibrium gas [5]. The subscripts '*i*' ranges from 1 to *N*+2, where *N* is the number of layers of MLI. Subscript 1 will refer to radiation shield and subscript *N* refers to cryostat inner wall. $p_{ins,i}$ is obtained using equation (4), P_c and T_c being the chamber pressure and warm chamber temperature, respectively. This model takes into account the effect of thermal transpiration.

$$p_{ins,i} = p_c\left(\frac{T_{ins,i}}{T_c}\right)^{1/2} \tag{4}$$

where,

$$T_{ins,i} = \frac{T_i + T_{i+1}}{2}$$

The gas heat conduction in viscous and transition region is calculated using equation (5) [8].

$$Q_{cond,i} = \frac{\kappa\left(T_{i+1} - T_i\right)}{\left(D + 2L\right)} \tag{5}$$

where, κ is the heat conductivity of the gas, *D* is the typical distance between two surfaces and *L* is the characteristic distance relating the mean free path of the gas of the gas molecules. The total heat transfer through the layers is obtained by adding the heat transfer by gas conduction and radiation.
The following assumptions have been made:

- The emissivities of stainless steel cryostat wall, copper radiation shield and MLI are 0.1, 0.15 and 0.07 respectively.
- Accommodation coefficient varies linearly from 1.0 at 80K to 0.8 at 300K for air [7].
- Area of MLI layer closest to the radiation shield is equal to the area of the radiation shield itself and for the successive layers of the MLI the area increases marginally and is same as the area of the first layer of MLI.

Radiation shape factors and thermal conductance are used for evaluating radiation heat transfer and gas conduction heat transfer.

$$F_{i,i+1} = \frac{1}{\left[\frac{1}{\varepsilon_i} + \frac{A_i}{A_{i+1}}\left(\frac{1}{\varepsilon_{i+1}} - 1\right)\right]} \tag{6}$$

$$\Lambda = \left(\frac{\gamma + 1}{\gamma - 1}\right)\sqrt{\frac{R}{8\pi T_{ins}}} \tag{7}$$

The radiation heat transfer and gas conduction heat transfer equations can then be written as in equation (11) and (12). The total heat transfer through i^{th} layer will be sum of the two modes of heat transfer.

$$Q_{rad,i} = \sigma A_i F_{i,i+1}\left(T_{i+1}^4 - T_i^4\right) \tag{8}$$

$$Q_{cond}, i = \Lambda p_{ins,i}\left(T_{i+1} - T_i\right)A_{i+1} \tag{9}$$

Fig. 2 shows the calculated variation of total heat transfer with the chamber pressure for 0, 10, 20 and 30 layers of MLI considering the different heat transfer mechanisms considered in equations (5), (8) and (9). It is observed that by the use of MLI the total heat transfer is reduced by up to 27 times. Figure 3 shows the variation of rate of heat transfer with number of MLI layers at a pressure of 0.1 Pa for the different heat transfer mechanism: radiation, gas conduction and combined gas conduction and radiation. Figure 4 shows the temperatures of the thirty layers of MLI for the different modes of heat transfer. Temperatures of the upper curve are calculated by restricting the heat transfer to radiation, lower curve are calculated by restricting the heat transfer to gas conduction. The middle curve is obtained by considering both radiation and gas conduction. The temperature gradient is high near the cold boundary; consequently the gas conduction increases and the radiation heat transfer decreases when approaching the cold wall. The highest temperature difference and consequently the highest heat transfer rate is calculated between the radiation shield and the adjacent MLI layer.

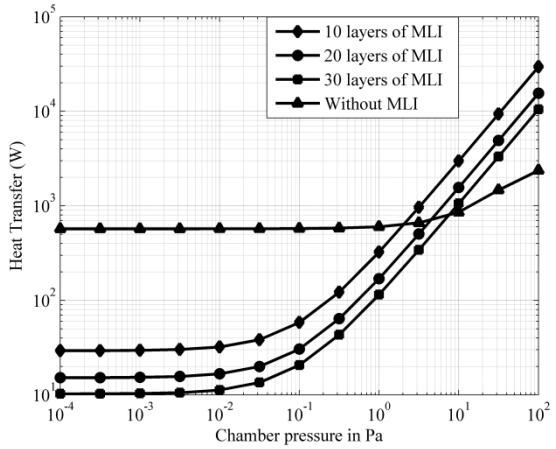

Fig. 2. Relationship between Heat Transfer rate and the chamber pressure for 0, 10, 20, 30 layers of MLI

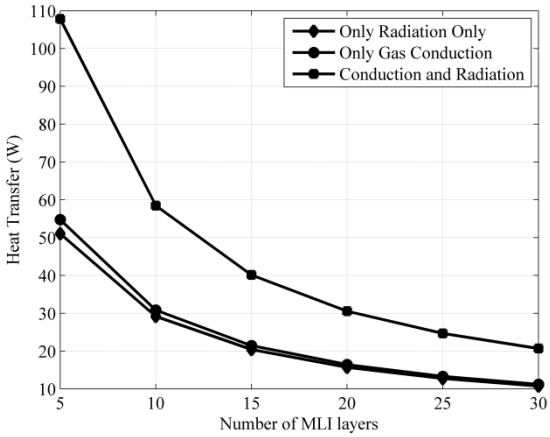

Fig. 3. Calculated Variation of heat leak with number MLI layers

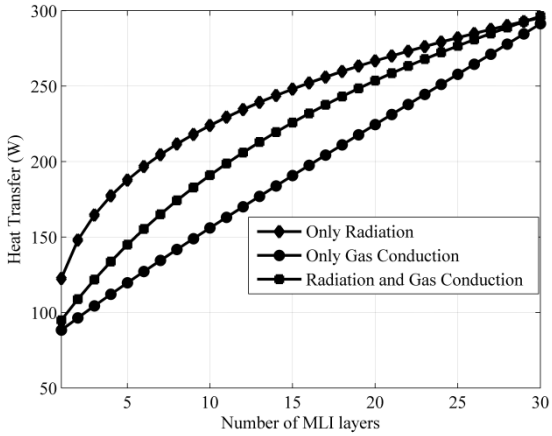

Fig. 4. Calculated temperatures of 30 layers of MLI considering different heat transfer mechanism

3. Vacuum in the Cryostat

From the results of heat transfer in the cryostat (Fig. 2) it is seen that the upper limit of the pressure in the cryostat can be set at 0.1 Pa as the total heat transfer rate with 30 layers of MLI is about 21 Watts. In view of the large size and weight of the magnet, a seal off approach might not be operationally feasible and the option of continuous pumping of the cryostat is considered. The internal volume of the cryostat is 1.84 m^3. Total internal surface area of the cryostat, the helium vessel, the beam tube, and other SS elements sums up to 39 m^2. The surface area of the thermal shield (both internal and external surfaces) is 37 m^2. The G10 epoxy material surface area is 1.9 m^2. Table 1 tabulates the area and the outgassing rates of the materials after 1 hr in vacuum. The outgassing rates are taken from the references [9, 10]. The total outgassing load was found to be 6.74 Pa l/sec.

Table 1: Outgassing rates of material inside the cryostat

	Material	**Surface Area (m^2)**	**Outgassing rate (Pa.l/sec/cm^2)**	**Estimated gas load (Pas.l/sec)**
Cryostat+Beam Tube+He Vessel	SS	39	1.20E-05	4.68
Radiaion Shields	Copper	37	5.30E-06	1.96
Support Links	G10	1.9	1.33E-06	2.49×10^{-02}
MLI	Mylar	888.68	8.50E-09	7.55×10^{-02}

An effective pumping speed of 90 liter/sec is expected to achieve a pressure better than the operating pressure. However, degassing/ vacuum baking of the system is required in order to achieve a better vacuum in short time. Taking the outgassing rates for the degassed materials from [9], a pressure of 1×10^{-3} Pa can be achieved.

4. Preliminary Design of the Vacuum System for Vacuum System for FAIR Super FRS Quadrupole Magnet Cryostat

Considering the effect of stray magnetic field the pumping system for the FAIR Super FRS Quadrupole Magnet system will be located at a distance of 1.5 meter from the central position and connected to the cryostat via a 100 mm diameter vacuum duct. The conductance of the vacuum duct will be 121 liter/sec. A dry mechanical pump of speed 210 liter/min will be used for the rough pumping of the cryostat from atmosphere. A turbomolecular pump of 350 liter/sec pumping speed will be used for attaining the base pressure. The expected pump down time from the atmosphere to 0.01 Pa by the pumping system is evaluated by solving mass balance equation (10). It was found that a pumping time of about 2 hr and 25 minutes will be required. Figure 5 shows the expected pump down curve for cryostat vacuum system.

$$\overline{Q} = SP + V\frac{dP}{dt} \tag{10}$$

Where $\overline{Q}$ is the gas load to the cryostat vacuum system obtained by adding the outgassing contributions from the different materials inside the cryostat, *S* is the effective pumping speed, *V* is the volume of the vacuum space and *P* is the pressure inside the cryostat. The outgassing from the surface varies depends of times after the start of pumping, expressed as in equation (11) [11].

$$\overline{Q} = K_1 t_h^{-\lambda}$$

Where K_1 is the outgassing rate at one hour.

Figure 5 shows the expected pump down curve for unbaked cryostat vacuum system. To reduce the pump down time rough pumping of the cryostat at elevated temperatures is required.

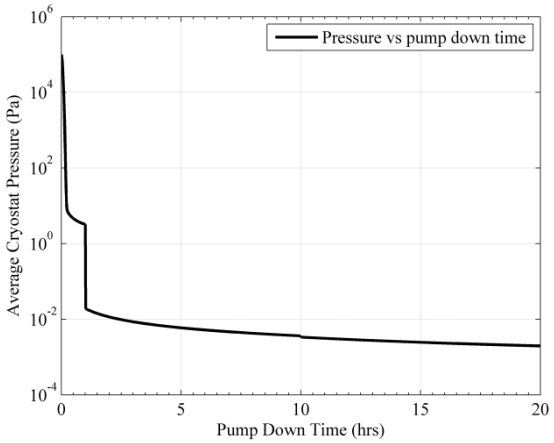

Fig 5. Expected Pump Down curve the Quadrupole Magnet Cryostat Vacuum system

5. Summary

The heat transfer in the FAIR Super FRS Quadrupole magnet cryostat was discussed and the required vacuum was evaluated. The vacuum system that will achieve the required vacuum and hence minimize the heat transfer has been discussed. Since the outgassing within the cryostat cannot be negligible, the pressure in the system may be determined by the gas load. Hence it is important to determine the outgassing rates of the materials present inside the cryostat at 300K. Further the need for degassing the cryostat is discussed for improving the pump down time of the cryostat.

References

[1] G. Pal, U. Bhunia, J. Akhter, C. Nandi, A. Datta, P.R. Sarma, S. Roy, S. Bajirao, S. Bhattacharyya, T.K. Bhattacharyya, M.K. Dey, C. Mallik and R.K. Bhandari. Superferric quadrupoles for FAIR Super FRS energy buncher, Cryogenics, ACASC 2011 Conference Proceedings in print.

[2] "Design of Outer Vacuum Chamber for Long Superconducting Quadrupoles for Fair Super FRS Energy Buncher", J. Akhter, G. Pal, C. Nandi, S. Roy, U. Bhunia, A. Datta and C. Mallik, presented at ACASC 2011, New Delhi. Indian Journal of Cryogenics in print.

[3] C. K. Krishnaprakas, K. Badari Narayan, Pradip Dutta. Heat Transfer Correlations for Multilayer Insulation system. Cryogenics Volume 40 (2000) 431-435.

[4] Cunnington GR, Tien, CL. A study of heat transfer processes in multilayer insulation. In: Bevans JT, editor. Thermophysics: application to thermal design of spcaecraft, AIAA progress in astronautics and aeronautics, vol. 23. New York: Academic Press; 1970. O. 111

[5] R. J. Corroccini. Gaseous Heat Condcution at low pressures and Temperatures, Vacuum, Vol. 7 and 8; 1957-1958.

[6] T. Nast. Radiation Heat Transfer in Handbook of Cryogenic Engineering: Taylor and Francis; p 186-202.

[7] R.B. Scott, Cryogenic Engineering, Met-Chem Research, 1963.

[8] A. Roth. Vacuum Technology. North-Holland Publishing Company. 1976

[9] R. J. Elsey. Outgassing of vacuum materials-II, Vacuum, Vol. 25, Number 8, 1975.

[10] A. P. M. Glassford and C. K. Liu. Outgassing rate of Multilayer Insulation, Lockheed Palo Alto Research Laboratory

[11] O'Hanlon, John F., A User Guide To Vacuum Technology, John Wiley and Sons, 1980